PCCP

Accepted Manuscript

ROYAL SOCIETY OF CHEMISTRY

www.rsc.org/pccp

Physical Chemistry Chemical Physics
CREATED USING THE RSC LaTeX PCCP ARTICLE TEMPLATE – SEE www.rsc.org/electronicfiles FOR DETAILS
ARTICLE TYPE www. rsc.org/xxxxxx | XXXXXXXX

Competition direct vs indirect photochromism dynamics in constrained inverse dithienylethene molecules†

Aude Lietard[a,b,c], Giovanni Piani[a,b], Lionel Poisson*‡[a,b,c], Benoît Soep[a,b,c], Jean-Michel Mestdagh[a,b,c], Stéphane Aloïse[d], Aurélie Perrier[e], Denis Jacquemin[f,g], Michinori Takeshita[h]

Received Xth XXXXXXXXXX 20XX, Accepted Xth XXXXXXXXX 20XX
First published on the web Xth XXXXXXXXXX 200X
DOI: 10.1039/b000000x

State-of-the-art experimental and theoretical tools were used to investigate the gas-phase relaxation dynamics of various photoexcited photochromic dithienylethene molecules in situations were several relaxation channels are simultaneously at play. Unconstrained and constrained dynamics were addressed by considering unbridged and bridged molecules with a polyether bridge of various size (from 2 to 4 units). Time-resolved ultrafast ionization spectroscopy techniques were used to probe the dynamics. This revealed the existence of several relaxation pathways from the first excited state to the ground-state. Characteristic times were determined for each process. These channels are competing at an early stage of the dynamics only when the initial wavepacket splits in two parts. A striking excited state wavepacket oscillation is observed in bridged molecules. A general reaction mechanism is proposed which rationalizes the carbon-carbon distance rule which is widely used as an empirical tool to predict the photoactivity of photochromic molecules in crystals.

1 Introduction

A major part of the femtochemistry studies on isolated molecules in the gas phase, concerns situations where a series of non adiabatic events occur sequentially[1]. Although the number of degrees of freedom is significant in large organic molecules, a single process is often dominating each step of the sequential decay and competing relaxation processes can be neglected. Here, we aim at exploring a significantly different situation where parallel, and so competing, relaxation processes are simultaneously at play inside the same molecule. Although the present paper adopts a very general point-of-view with respect to parallel relaxation processes in molecules isolated in the gas phase, photochromic dithienylethene molecules will be considered in view of their practical impact. We consider indeed important to examine whether in the intrinsic dynamic of these molecules, the photochromic reaction pathway is in competition with relaxation pathways which reduce the photochromic yield.

The IUPAC Technical Report on "Organic Photochromism"[2] defines photochromism as a reversible transformation of chemical species induced in one or the reverse direction by absorption of electromagnetic radiation between two forms, A and B, each one having a different absorption spectrum. Photochromic molecules present various optoelectronic applications such as optical memories and optical switches[3].

Normal dithienylethene (N-DTE) and its substituted derivatives are often used as photochromic organic compounds. Numerous studies in condensed phases, solutions[4–6] or crystals[7,8], have revealed their outstanding properties: *e.g.* weak photodegradation, excellent thermal stability and high photoconversion yield. Theoretical investigations are also available[9–13]. The photochromic reaction pathway of these molecules corresponds to a switch between an open form (OF) and a closed form (CF) through a photoinduced electrocyclization process. The ring closure reaction is initiated by UV radiation while the reverse process occurs upon visible irradiation. The time scale of the OF-CF photoconversion falls in the picosecond range and varies with the molecular structure[14,15]. In crystals[16,17], the photochromic yield is strongly dependent on the distance between the two carbon atoms which participate in the photocyclisation, hence offering a qualitative tool

† Electronic Supplementary Information (ESI) available: Full tables, molecular orbitals. See DOI: 10.1039/b000000x/

[a] *CNRS, IRAMIS, SPAM, Laboratoire Francis Perrin, URA 2453, 91191 Gif-sur-Yvette, France.*
[b] *CEA, IRAMIS, SPAM, Laboratoire Francis Perrin, URA 2453, 91191 Gif-sur-Yvette, France.*
[c] *Université Paris Sud 11 - ED470 Chimie de Paris Sud, 91450 Orsay CEDEX, France.*
[d] *Université Lille 1 - LASIR UMR 8516, 59655 Villeneuve d'Ascq CEDEX, France.*
[e] *Université Paris 7 - Sorbonne Paris Cité - ITODYS UMR 7086, 75205 Paris CEDEX, France.*
[f] *Laboratoire CEISAM - UMR CNRS 6230, Université de Nantes, 2 Rue de la Houssinière, BP 92208, 44322 Nantes Cedex 3, France*
[g] *Institut Universitaire de France, 103 Boulevard Saint Michel, 75005 Paris Cedex 5, France*
[h] *Department of Chemistry and Applied Chemistry, Faculty of Science and Engineering, Saga University, Honjo 1, Saga 840-8502, Japan*
‡ email address: lionel.poisson@cea.fr

to rationalize photochromic efficiencies in view of applications.

The present paper addresses a slightly different class of molecules, derivatives of inverse dithienylethene (I-DTE), where a photoconversion between OF and CF is also responsible for the photochromic property. The OF and CF of I-DTE molecules are shown in Figure 1. I-DTE differs from N-DTE by the bond location between the lateral thienyls substituents and the perfluorocyclopentene ring. It is in β of the sulfur atom in N-DTE whereas it is in α position in I-DTE. The latter configuration offers more flexibility to synthesize substituted I-DTE molecules[18]. I-DTE hence appears as the photochromic core of a new class of photochromic compounds which have not received yet as much attention as N-DTE molecules. The similarities and differences between I-DTE and N-DTE systems have been explored in several works[9,13,18–22].

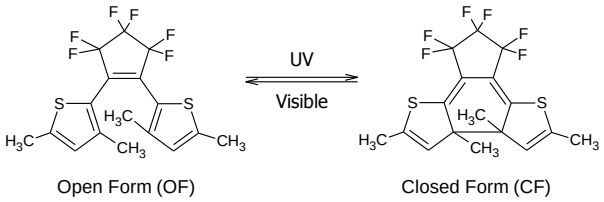

Fig. 1 Photochromic reaction of I-DTE.

The dithienylethene OF (both N-DTE and I-DTE) presents two conformations, that are distinguished by the parallel (called P conformer of pseudo-Cs symmetry) or antiparallel (AP conformer of pseudo-C2 symmetry) orientations of the thienyl groups. Condensed phase experiments on N-DTE revealed a very slow internal conversion between the two conformers with a much larger timescale than μs[4]. This suggests that the P and AP conformers are separated by large energy barriers. A lower barrier was observed for I-DTE[9]. The fact that the P conformer, where the thienyl groups do not have the proper orientation for the photocyclisation reaction, has no photochromic property is an indication that the landscape in the excited potential energy surface (PES) is also fairly complicated with basins and energy barriers which prevent finding the photochromic pathway to CF within the lifetime of the excited state. The existence of a non-reactive conformer is an important issue for the practical use of DTE molecules. Bridged variants of the I-DTE molecules have been synthesized, named I-DTE-O$_x$ with $x = 2,3,4$, in order to lock the ground state I-DTE core with the reactive geometry (AP conformer), they are shown in Figure 2 together with unbridged I-DTE molecule. Other kind of I-DTE bridged molecules with chiral bridges were synthesized and NMR studies were done, which showed that 100 % of these bridged molecules are locked in the AP conformer in $CDCl_3$ solvent[20]. In the present work I-DTE-O$_x$ molecules are isolated in the gas phase, and we anticipate that the efficiency of bridges in these molecules may be reduced due to the flexibility of the bridge.

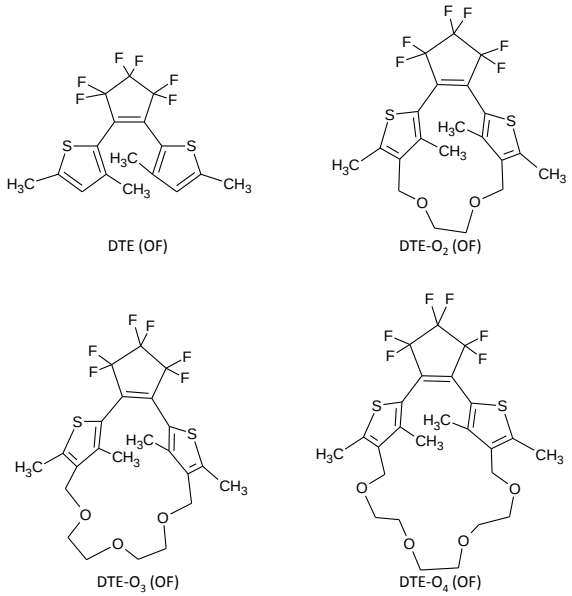

Fig. 2 Opened forms of basic and bridged molecules.

We mentioned above that the excited PES landscape in N-DTE is fairly complicated, this must be the case in I-DTE also. In the perspective of femtochemistry studies which are at the center of the present work, the presence of multiple energy basins and barriers may result into a splitting of the initial wavepacket and evolution along relaxation pathways which compete together. This offers a unique benchmark to explore dynamical regimes involving parallel relaxation pathways. The present experimental work complemented by theoretical calculations considers the I-DTE and I-DTE-O$_x$ molecules, shown in Figure 2, isolated in the gas phase. The basic idea is to launch the photochromic I-DTE core in different regions of the excited PES to explore how subsequent dynamics is affected by the initial geometry. Since the Franck-Condon principle precludes varying the region of excitation, the series of I-DTE-O$_x$ bridged molecules is used to create a variety of initial geometries around the AP conformer and to observe the competition between the photochromic reaction pathway with non reactive pathways.

On the experimental side, the gas phase reaction dynamics of I-DTE and I-DTE-O$_x$ molecules is explored using the femtosecond pump-probe approach in a detection scheme which couples photoelectron spectrometer and ion mass spectrometry. This documents directly the relaxation of the initial electronic excitation within electronic states as a function of the time delay between the photoexcitation pump and

photoionization probe. The interpretation of these results is supported by density functional theory (DFT) and time dependent-DFT (TD-DFT) calculations which overview the isomers which can be present in the experiment and document their excitation and ionization energies. Beside revealing the evidence of parallel relaxation pathway, joint experiment/theory allows us proposing a general model which accounts for the cyclisation reaction mechanism in isolated I-DTE compounds.

2 Experimental details

The setup used for the present femtosecond pump-probe experiments has been described elsewhere[23,24] and is schemed in Figure 3. Shortly a pulsed valve operating at 20 Hz creates a supersonic jet in the source chamber ($P_{source} \sim 10^{-5}$ mbar). Helium is used as the carrier gas at a pressure of *ca.* 2 bars. An oven is mounted on the orifice plate of the valve. The solid sample is introduced in the oven and maintained at a temperature between 320 K and 350 K, below the limit of the decomposition of the molecule which is to be evaporated. The latter is checked experimentally by mass spectrometry.

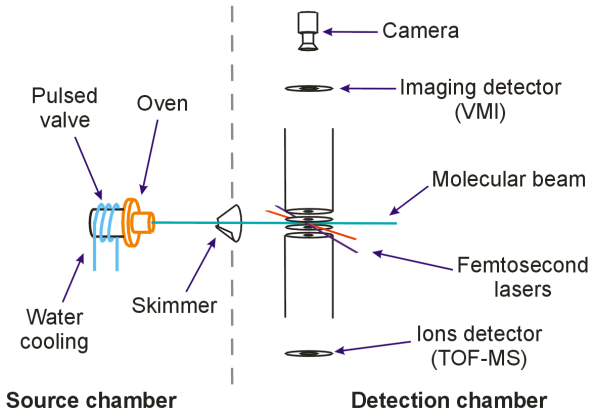

Fig. 3 Schematic of the experimental setup.

After passing through a 1 mm diameter conical skimmer, the molecular beam enters in the detection chamber ($P_{detection} \sim 10^{-7}$ mbar) where it crosses perpendicularly the pump and probe femtosecond laser beams. The pump laser wavelength is the third harmonic of a Ti:Saphire laser and was measured at 265 nm, with a $\sim$ 3 nm full-width-at-half-maximum (fwhm). The probe laser wavelength was measured at 795 nm (Ti:Saphire laser), with a $\sim$ 20 nm fwhm. The measured cross correlation between the laser pulses is 120 fs. The probe pulse is delayed by a variable time with respect to the pump pulse. The pump-probe delay is varied up to 60 ps enough to cover the entire dynamics.

The probe operates by multiphoton ionization. The resulting photoions (PI) and photoelectrons (PE) are extracted along a vertical axis. The PI are monitored by a Time-Of-Flight Mass Spectrometer (TOF-MS) and the PE are monitored independently using a Velocity Map Imaging (VMI) device[25] which documents their kinetic energy and angular distribution.

Raw images of the 2D projection of the PE distribution are recorded by a CCD camera. To recover the 3D distribution, they are inverted according to the pBASEX algorithm[26] using the LV_pBASEX inverse Abel Transform software[27]. Since raw images suggest an isotropic distribution of the PE, the inversion procedure was limited to an isotropic decomposition. The energy calibration of the image was provided by the multiphoton ionization of the oxygen molecule[28,29].

The I-DTE derivatives used in the present work (see Figure 2) were synthesized and purified as described by Takeshita M. *et al.*[18]. I-DTE 1,2-bis(3,5-dimethyl-2-thienyl)perfluorocyclopentene features the photochromic core which is presented in the bridge molecules. The latter are constrained with a polyether bridge and are named I-DTE-O_x where x corresponds to the number of oxygen in the polyether bridge.

3 Computational methods

The photochromic core of the I-DTE molecules is composed of three rigid rings. Hence, a reduced number of flexible coordinates needs to be explored to identify the possible conformers. Nevertheless, due to the flexibility of the polyether bridge a large number of rotamers is accessible to the bridged I-DTE-O_x molecules. For this reason, a two-step protocol was used to explore the ground state PES. In the first step, molecular dynamics (MD) simulations were performed to identify a panel of structures and the results reflect the chemical intuition (see the Electronic Supplementary Information, ESI, for details). At this stage, various conformers, including P and AP conformers were identified. In the second step, molecular structures, selected from MD trajectories, were optimized using the Gaussian 09 package[30]. These optimizations have been performed both for the ground-state (S_0) and excited-state (S_n) using DFT and TD-DFT approaches, respectively. The 6-31G+(d) atomic basis set was used since it was found to yield valuable results for both the geometrical and optical properties of a rich variety of conjugated molecules[31]. Because of the size of these molecules the calculation was limited to I-DTE-O_x, x $\leq$ 3.

In line with previous DFT calculations dedicated to N-DTE[9], the minima of the S_0 and S_n PES of the I-DTE-$O_{2,3}$ molecules have been determined using the ωB97X range-separated hybrid functional[32,33]. Unlike to conventional hybrid functionals, these hybrids avoid the common overtwisting problem of the excited-state structure[31] and produce valid S_n geometries.

A tight convergence criteria (residual RMS force smaller than 10^{-5} a.u.) was used. Hereafter, the $S_{n,opt}$ geometry refer to the structure of the molecule optimized in the S_n state. To ascertain the nature of the optimized structures, vibrational frequencies have been systematically computed using analytical and numerical derivatives for the S_0 and S_n critical points, respectively.

The PBE0 hybrid functional has been used to determine the UV-Vis optical properties[34,35]. It was chosen for its fast and accurate predictions of the absorption and emission properties of I-DTE in condensed phase[9].

The calculations results are detailed in the ESI where optimized geometry of the conformers are given together with vertical and adiabatic transition energies to the first lowest excited states. Informations on theoretically determined ionization energies are also provided in ESI. Results which are directly relevant to the present experimental work are listed in Table 3.

4 Experimental results

4.1 Photoelectron

PE images were recorded up to a pump-probe delay of 60 ps for I-DTE and I-DTE-$O_{2,3}$ molecules. After inversion, the radial distribution in each image reflects a PE spectrum. Given the measured signals are fairly low, the section below reports various summations within these spectra to get reliable information.

4.1.1 Summed photoelectron spectra: To increases substantially the signal/noise ratio and to identify clearly the shape of PE spectra, all those performed at various pump-probe delays are summed together. Summed spectra are shown in Figure 4 for I-DTE and I-DTE-$O_{2,3}$. The PE signal is too low with I-DTE-O_4 to deserve a reliable PE spectrum. This is due to a very small lifetime of the product under the temperature conditions in the oven which cannot be compensated by using large product quantities, given the low yield of its synthesis.

Although broad and apparently structureless, the spectra in Figure 4 can be decomposed as a combination of two exponential decay functions and a Gaussian function centred about 0.6 - 0.7 eV which mimics a broad peak. Nevertheless, a single exponential decay is observed in the middle panel for I-DTE-O_2 and the Gaussian peak is visible for I-DTE and I-DTE-O_2 only. The fit parameters which define the exponential decay and Gaussian functions are reported in Table 1. Given the location of the black arrows in Figure 4, the broad Gaussian peak can be assigned to a 3 probe photon ionization of the S_1 state in the $S_{0,opt}$ geometry, *i.e.* prior to any structural relaxation.

4.1.2 Time resolved photoelectron signals: Summation over the radial distribution in each image leads to the total PE signal as a function of the pump-probe delay. It is shown in Figures 5 up to 6 ps and in the inserts up to 20 ps. For each molecule, a multiexponential evolution is observed: first, a rapid decay (few hundred of femtoseconds); then a longer one (few picoseconds); finally the signal does not go to zero at very long time scales (see inserts at $\sim$ 20 ps) and stabilize to $\sim$ 5-10% of the maximum. The PE signals in Figure 5 were fitted by two exponential decay functions $\left(\exp\left(-\frac{t}{t_i}\right) \text{ with } i = 1,2\right)$ convoluted by the cross correlation function of the pump and probe laser pulses. For reasons that will appear later, the plateau is represented by a step function at time zero, also convoluted by the cross-correlation function. The time constant of the exponential functions is given in the top of Table 2 for each molecules. The interpretation model which justifies this fit is presented later.

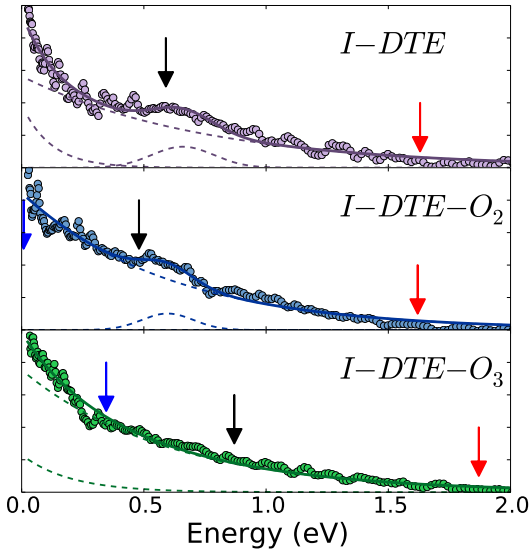

Fig. 4 Summed PE spectra. The dotted lines represent the contributions to the fit performed with the parameter listed in Table 1. The arrows indicate the maximum PE energy expected from a vertical [1 pump + 3 probe photon] ionization scheme from the S_0 optimized geometry $S_{0,opt}$ (in red); from a 3 probe photon ionization of the S_1 state with the $S_{0,opt}$ geometry (in black); and from a 3 probe photon ionization of the S_1 state with the $S_{1,opt}$ geometry (in blue) (out of the figure range for I-DTE in the top panel). The arrows were located with the theoretical calculations reported in Section 3.

4.1.3 Time resolved PE signal at low and high PE energies: When inspecting the PE images recorded at pump-probe delays between 0 and 60 ps, the shape of the PE spectra does not change significantly, and do not need to be presented thoroughly. However, the behavior at time delay below 1 ps reveals small differences, at the limit of sensitivity of the experiment, when comparing the PE signals corresponding to low (< 0.25 eV) and high (> 1.2 eV) PE kinetic energies. Evolu-

	Exponential 1	Exponential 2	Gaussian		Max E_{PE} from $S_{0,opt}[1,3']$	Max E_{PE} from $S_{1,opt}[3']$
	E_1 (eV)	E_2 (eV)	fwhm (eV)	E_0 (eV)	(eV)	(eV)
I-DTE	0.120	0.750	0.180	0.660	1.63	0.59
I-DTE-O_2	-	0.600	0.150	0.600	1.62	0.48
I-DTE-O_3	0.200	0.600	-	-	1.87	0.87

Table 1 Parameters defining the two exponential decay $\left(\exp\left(-\frac{E}{E_i}\right)\right)$ and the Gaussian $\left(\exp\left(-\frac{(E-E_0)^2}{fwhm^2}\right)\right)$ functions used to fit the PE spectra displayed in figure 4. The last two columns give the location of the red and black arrows in figure 4 (E_{PE} is the expected energy of the ejected PE. [X,Y'] correspond respectively to the number of pump and probe photon).

	I-DTE	I-DTE-O_2	I-DTE-O_3	I-DTE-O_4
t_1	170 ± 4 fs	290 ± 3 fs	200 ± 3 fs	120 ± 5 fs
t_2	3.8 ± 0.1 ps	3.70 ± 0.01 ps	6.80 ± 0.03 ps	1.75 ± 0.04 ps
Period	-	1.03 ± 0.01 ps	1.20 ± 0.03 ps	1.1 ± 0.1 ps

Table 2 Relaxation time constants of I-DTE, I-DTE-O_2, I-DTE-O_3 and I-DTE-O_4 from the PE signal and oscillation period of each bridged molecules from the TOF signal.

tions of the PE signals as a function of the pump-probe time delay are reported in Figure 6. The raising time of the low energy signal (in purple) is apparently slower by $\sim$ 25 fs in I-DTE and I-DTE-O_3. This corresponds to a 25 fs delay to reach the maximum, and this extra delay show up also in the decay after the signal has reached its maximum.

4.2 Photoion experiments

4.2.1 Mass spectra: Time-of-flight (TOF) mass spectra have also been collected for each molecule as a function of the pump-probe delay. Figure 7 shows the sum of all TOF spectra recorded during an experiment. In each spectrum, the parent mass is assigned to the the narrow peak with the characteristics sulfur and carbon isotopic distribution. Fragment peaks are observed at lower masses. They are broader than the parent peak, due to the recoil velocity along the fragmentation coordinate. Note that the fragmentation likely occurs during the ionization process, when the absorption of extra photons above the ionization limit gives enough internal energy to stimulate its fragmentation [23].

The parent peak is observed at 396, 482, 526 and 570 amu in the mass spectra of I-DTE, I-DTE-O_2, I-DTE-O_3 and I-DTE-O_4, respectively. No other intense narrow peak is observed, indicating both the purity of the sample used in these experiments and the absence of the thermal degradation in the oven. Nevertheless, impurities are observed in small quantities with I-DTE-O_2, they are labeled with stars in the figure.

A very small fragmentation is observed with I-DTE, compared to the other molecules. The fragments correspond to a loss of methyl groups. For the three bridged molecules, fairly large

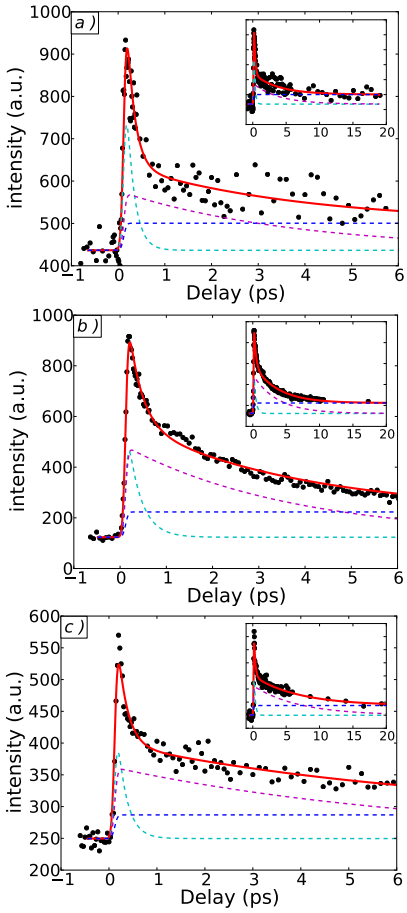

Fig. 5 Total PE signal as a function of the pump-probe delay for the I-DTE (a), I-DTE-O_2 (b) and I-DTE-O_3 (c) molecules. The pump and probe wavelengths are 265 and 795 nm respectively. The full curve running through the experimental points is a fit using the parameters listed in Table 2. The dashed curve shows the contribution of the two exponential decays and step function used in the fit (see text for details).

intensity fragments are measured at 394, 409 and 424 amu. They correspond to the partial or total loss of the polyether bridge. No other fragment is observed with I-DTE-O_3 and I-DTE-O_4. In contrast a close inspection of I-DTE-O_2 spectrum reveals barely visible fragments between 300 and 370 uma. Another fragment, which does not appear with the scale of the Figure 7 is also observed at 60 amu for I-DTE-O_2. It corresponds to the ionized polyether bridge.

4.2.2 Time resolved PI signals: The intensity of each peak in the above mass spectra was monitored as a function of the pump-probe delay. Summing the signal for all fragments lead to the full PI signal. It has been checked that its time dependence has the same shape as observed in Figure 5 for the corresponding PE signals. Since no charged particule,

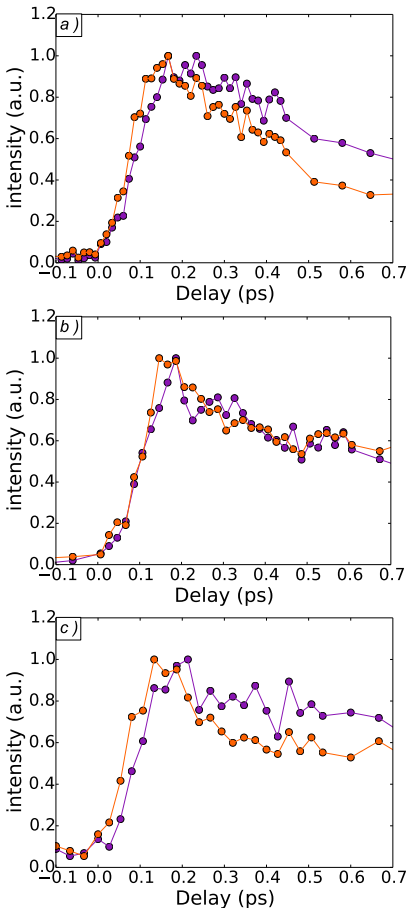

Fig. 6 PE signal corresponding to low (< 0.25 eV, in purple) and high (> 1.2 eV, in orange) PE kinetic energy as a function of the pump-probe time delay for the I-DTE (a), I-DTE-O_2 (b) and I-DTE-O_3 (c) molecules. The pump and the probe wavelengths are at 265 and 795 nm respectively.

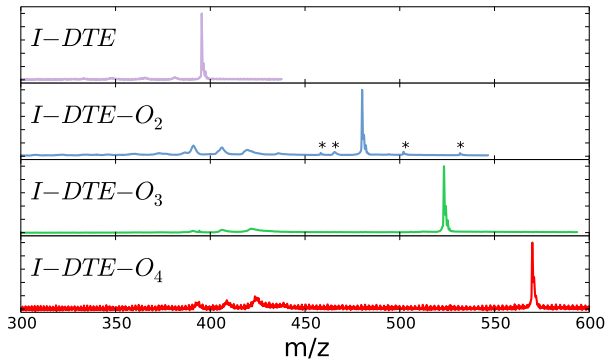

Fig. 7 Mass spectrum of the I-DTE, I-DTE-O_2, I-DTE-O_3 and I-DTE-O_4 molecules as labeled in the figure. Peaks marked with an asterisk (*) are due to impurities.

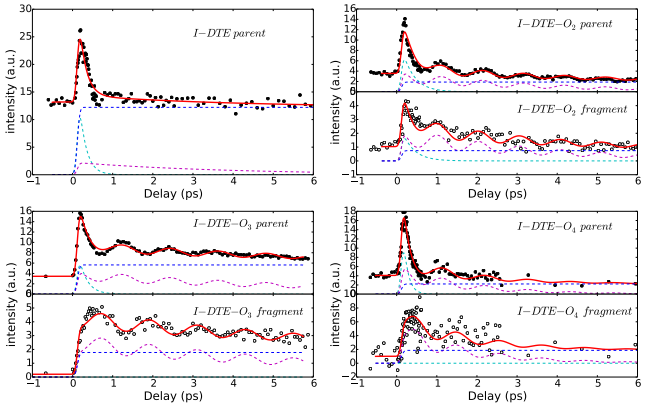

Fig. 8 Ion peak intensity as a function of the pump-probe time delay as labelled in the figure. The pump and the probe wavelengths are at 265 and 795 nm respectively. The full line is a fit running through the experimental points and the dotted lines are the contributions (see text for details).

electron or ion, is lost in the detection, the full PI signal is indeed the exact counterpart of the PE signal.

Time dependent PI signals are shown in Figure 8 for a few peaks: the I-DTE, I-DTE-O_2, I-DTE-O_3, I-DTE-O_4 parents and for the bridged molecules, the fragment of largest mass ($m/z = 424$). As observed in Figure 5 for the PE signals but with different ratio, a rapid decay is followed in each parent peak by a longer decay. The very striking observation with the bridged molecules is that an oscillation regime, which does not show up at first glance in the PE signals, is superimposed to the longer decay for both the parent and the fragment. Apparently in-phase oscillations are observed between the parent and fragment of I-DTE-O_2 whereas the oscillations are very distinctly out-of-phase for I-DTE-O_3. Given the signal/noise ratio, it is hard to conclude for I-DTE-O_4.

For technical reasons, it was not possible to reduce the 2-photon ionization of the parent molecule by the pump pulse alone. Hence, the parent peak intensity is not zero at negative time when the probe pulse precedes the pump pulse. In turn at positive time, both photo-excited and ionized parent molecules are present and interact with the probe pulse. The former lead to the time dependent signal and reflects the desired excited state dynamics of the parent molecule whereas the latter may absorb a probe photon and fragment subsequently. Calculations on the electronically excited I-DTE ions show indeed that energy levels are present in the 1 to 2 eV excitation range of the I-DTE-O_x ions. The excess energy due to the absorption of a probe photon (1.5 eV) may induce fragmentation, thus reducing the amont of parent ion. This explains why at long time delay, the parent ion signal goes below that measured at negative time. This effect is clearly observed for I-DTE-O_2 and I-DTE-O_4, barely visible for I-DTE

and not at all for I-DTE-O_3. Since the 2-pump-photon ionization is likely to form the molecular ion out of its equilibrium geometry, the subsequent absorption of a probe photon can depend on the pump-probe delay and include a damped oscillation regime, due to the structural relaxation of the molecular ion about its equilibrium geometry. When observed, *i.e.* for I-DTE-O_2 and I-DTE-O_4, this effect is superimposed to (and likely hard to disentangle from) the time depend photoionization signal which reflects the excited state dynamics of the parent molecule.

5 Data analysis and discussion

5.1 Initial excited state

Molecule	State	Excitation energy (eV)	f	State description
I-DTE	S_1	3.63	0.28	HOMO $\rightarrow$ LUMO
	S_2	4.23	0.07	HOMO-1 $\rightarrow$ LUMO
	S_3	4.45	0.06	HOMO-2 $\rightarrow$ LUMO
	D_0	7.72	-	-
I-DTE-O_2	S_1	3.53	0.15	HOMO $\rightarrow$ LUMO
	S_2	4.16	0.05	HOMO-1 $\rightarrow$ LUMO
	S_3	4.31	0.04	HOMO-2 $\rightarrow$ LUMO
	D_0	7.73	-	-
I-DTE-O_3	S_1	3.67	0.34	HOMO $\rightarrow$ LUMO
	S_2	4.27	0.07	HOMO-1 $\rightarrow$ LUMO
	S_3	4.35	0.01	HOMO-2 $\rightarrow$ LUMO
	D_0	7.48	-	-

Table 3 Vertical excitation energy calculated at the TD-PBE0/6-31+G(d)//ωB97X/6-31+G(d) level for OF-AP conformer in the $S_{0,opt}$ geometry, corresponding oscillator strengths f and state description. D_0 is the ground state of the ion. The complete table is presented in the ESI.

Table 3 indicates that the transition to the S_1 state of the OF-AP conformers of I-DTE, I-DTE-O_2 and I-DTE-O_3, presents a strong oscillator strength and corresponds to a HOMO $\rightarrow$ LUMO electron promotion. In contrast, transition to S_2 and S_3 states present smaller oscillator strengths, reduced by a factor 4. Hence, the pump pulse at 265 nm ($\sim$ 4.6 eV) is likely to populate the S_1 state rather than S_2 or S_3 although it has enough energy to promote transitions above S_3 state.
The molecular orbitals corresponding to the S_0-S_1 excitation are shown in the ESI. Their shape is typical of open-ring dithienylethenes[36] and indicates that the electronic excitation corresponds to a transitions of $\pi\pi^\star$ character mainly localized onto the double bonds of the central ring. It has been shown that such a characteristics is required to induce the cyclisation reaction which is responsible for the photochromic property of DTE[37].

5.2 Gas phase dynamics: an enhanced complexity

Four dynamical features characterize the gas phase dynamics of I-DTE and I-DTE-O_x: two time constants in the order of 120-290 fs, 1-7 ps and a plateau which might reflect a very slow decay in the $\gg$ 100 ps regime. These three dynamical features might be compared to decays observed in Isibashi *et al.*[4] and Sangdeok *et al.*[6] time resolved studies in the condensed phase. A fourth, very important dynamical feature exists in the gas phase dynamics of bridged I-DTE-O_x molecules: an oscillation regime which is superimposed to the few picosecond delay. These 4 dynamical features are discussed hereafter.

5.2.1 Two competitive relaxation mechanisms: The photochromism of dithienylethene molecules is associated with the photoinduced electrocyclization reaction schemed in Figure 1. The distance between the two C-atoms forming the CC bond during the cyclisation process is larger in the OF than in the CF. It appears as a convenient order parameter to examine the photoinduced OF-to-CF switch. We define as the "*OF-CF distance*" the distance between the two C-atoms involved in the σ-bond formation.
The OF-CF distance of the optimized S_0 state is larger than the one of the S_1 state. This suggests that slopes exist in the S_1 surface, which can move the molecule out of the Franck-Condon region of excitation and drive it to a region of shorter OF-CF distance. Note that the σ-bond is not formed at the geometry of the S_1 state. The two carbon atoms, which will be eventually bound together, are simply in better position to do so than at the S_0 equilibrium geometry. This suggests that the OF-CF distance cannot be identified directly as the reactive coordinate even if involved in the reaction mechanism. Likely, deformations along several coordinates associated with a non-adiabatic energy transfer to the ground state PES participate simultaneously to the photocyclisation process.
Calculations performed on a model skeleton of the I-DTE molecules showed that conical intersections (CI) exist between the S_1 and the S_0 PES which could drive a fast relaxation from the S_1 state to the ground state[10,13], finally promoting the electrocyclization reaction on the ground state surface. Importantly CI cannot be reached from the Franck-Condon region of the S_0-S_1 excitation by simply varying the OF-CF distance, but trough a multidimensional dynamics.
We have seen that the S_0-S_1 excitation corresponds to a $\pi\pi^\star$ transition localized on the C=C double bond of the central ring. An analogy can be drawn with the behavior of monoalkenes and cyclic alkenes. The $\pi\pi^\star$ excitation in these molecules results in a multidimensional dynamics where torsion about the C=C double bond is combined with pyramidalization about one of the carbon atoms. Then the molecule reaches a CI which funnels the electronic excitation as vibration of the ground state[38]. The same kind of behavior is

likely at play in the initial step of the excited state dynamics of the I-DTE and I-DTE-O_x molecules. Accordingly, the $\pi\pi^\star$ transition launches a vibrational wavepacket on the S_1 PES, which will undergo a multidimensional propagations, initially along torsion and pyramidalization coordinates. As it spreads on the excited PES, the wavepacket can reach the CI mentioned above. A rapid transfer to the ground state and subsequent photocyclisation would proceed. The faster time constant which appear in Table 2 documents the early dynamics of excited I-DTE and I-DTE-O_x molecules and must be assigned to this pathway. It falls in the 120-290 fs range for those molecules studied in the present work. This makes the initial step of the gas phase dynamics much faster by at least a factor 3 than observed in the condensed phase on BTF6[4]. This is probably realistic since this step involved large amplitude movements that are likely constrained and slowed down in the condensed phase.

As said in the Introduction, the majority of femtochemistry studies concerns a series of non-adiabatic events occurring sequentially. When a bi-exponential behavior is observed, the initial population rapidly decays into a level which decays more slowly. This picture does not apply here since S_1 is populated initially and the 120-290 fs time constants corresponds to a transfer to the ground state through a CI. The ionization potential of I-DTE and I-DTE-O_x molecules is too large indeed (see Table 3) to expect detection by the probe laser after the molecules have reached the ground state through the CI. We are left with the conclusion at this point that the excited state dynamics of these molecules is much more complicated than anticipated above, when comparing these molecules to mono-alkenes and cyclic alkenes. The number of deformation coordinates where the initial wavepacket can spread is indeed larger in the present case. Hence it is conceivable that a part of the wavepacket which does not find the CI at early time, spreads over deformation degrees of freedom which are not involved in the access to the CI. Hence, the time constant which falls in the 1.75-6.8 ps range in Table 3 is assigned to the evolution of this component of the wavepacket.

The picture with two parallel relaxation channels which emerges in the present gas phase experiment has been encountered also in condensed phase experiments that will be described elsewhere. It is discussed now in terms of coupling efficiency between vibrational modes. The two decays which appear in Table 3 are assigned to the reactive AP isomer, excited to the S_1 electronic state, but in two different classes of vibrational modes among those that are populated by vertical excitation from the ground state. Those associated with the movement toward the CI lead to the short time constant and the other modes to the long time constant. Actually this suggests that the two classes of modes are essentially uncoupled at a time scale of a few picoseconds corresponding to the slow time constant, otherwise intramolecular vibrational repopulation of the modes stimulating movement toward the CI would be at play and a single time constant would be observed. This seems surprising at a first glance, but the discussion of the oscillation regime in the next Section indicates that such mode uncoupling exists in the I-DTE-O_x molecules. Let us mention also that the existence of two relaxation pathways is supported by the calculations on the model diarylethene[10]. One can figure out that part of the wavepacket is composed by modes directly coupled to the ground state after the photoexcitation, whereas the other part is composed by other modes poorly coupled to the ground state and beating in the S_1 funnel. The observed decay figures out the coupling with modes involved in the CI and thus to the ground state. The separation of the modes in two operative classes has been involved very often in the radiationless decay of molecules to explain different dynamical behaviors operating in parallel[39].

5.2.2 The plateau observed after the transient decays: The energetics of the OF-AP and OF-P conformers of I-DTE which is provided by the DFT calculations, suggest a relative Boltzmann population at the nozzle temperature ($\sim$ 340 K) ranging between 75 % and 90 % in favor of the OF-AP conformer. At the final expansion temperature, 200 K, the AP:P ratio would reach 98:2. However, a supersonic expansions with helium as carrier gas is likely to freeze configurations rather than thermalizing them[40,41]. Hence, the actual conformer ratio is expected to be between the two limiting value, anyway strongly dominated by the photoactive OF-AP conformer. Nevertheless, this leaves a maximum of 25 % of the I-DTE molecule in the non-reactive isomer OF-P. Table 1 in the ESI indicates that the OF-P conformer can absorb the pump laser light at 265 nm. Hence, a possibility is that the plateau observed in I-DTE in Figure 5 (left panel) reflects the OF-P conformers which are present in the beam. The latter indeed would be excited by the pump laser at 265 nm and probed by multiphoton ionization by the probe laser at 795 nm as for the OF-AP conformer.

Figure 5 reveals also that a plateau exists for I-DTE-O_2 and I-DTE-O_3 in about the same amount as for I-DTE. At first glance, this could be attributed to the occurrence of OF-P conformers in the beam as just discussed for I-DTE. However this does not fit with NMR studies which showed that other kind of I-DTE bridged molecules with chiral bridges are present exclusively as the OF-AP conformer in $CDCl_3$ solvents[20], whereas the height of the plateau is about the same for the three molecules and represents $\sim$ 5-10% of the full signal. This might reveal that a suprathermal barrier exists between the two isomers which prevents their thermal equilibration in the condensed phase environment whereas the barrier would be accessible in the gas phase.

An alternative interpretation of the plateau in Figure 5 is provided by a theoretical investigation at the

CASPT2/CASSCF(10,10)/6-31G(d) level of the S_0, S_1 and S_2 surfaces of the N-DTE and I-DTE molecules[13]. It appears that a CI exists between the S_2 state of the OF-AP I-DTE conformer and the S_1 state of the OF-P I-DTE conformer which provides a downhill path from S_2 OF-AP I-DTE to S_1 OF-P I-DTE which is non-reactive. It was suggested in Section 5.1 that the excitation by the pump laser is toward S_1. Nevertheless the oscillator strength to S_2 and S_3 is only a factor 4 smaller than that to S_1. As the energy of the pump photon (4.68 eV) is large enough to reach the S_2 and S_3 levels, a small initial population into these states can be anticipated with the possibility that the downhill path mentioned above populates the non reactive S_1 OF-P I-DTE.

This alternative interpretation of the plateau in I-DTE can be extended to the I-DTE-O_2 and I-DTE-O_3 molecules. Hence we would be facing a third relaxation pathway of the initial wavepacket in parallel with the two that have been unraveled in the previous section. Of course, the energetics of this new pathway is very constrained to provide a downhill path from S_2 OF-AP I-DTE to S_1 OF-P I-DTE. Hence, we anticipate that the branching ratio to this relaxation pathway, *i.e.* height of the plateau with respect to the minimum intensity of the full signal, is very sensitive to the energy of the pump photon. Unfortunately with the present design of the laser facility, it was not possible to vary the excitation wavelength and to probe accordingly the presence of this new relaxation channel.

5.2.3 Oscillating wavepacket: The oscillation regime of bridged molecules is observed in the PI signal almost exclusively. This appears clearly when comparing Figures 5 and 8: large amplitude and fully resolved oscillations are observed in Figure 8. Only very dim oscillations, close to the experimental limit, are observed in Figure 5 for I-DTE-O_2 whereas the signal/noise ratio does not allow to conclude for the other bridged molecules. The oscillation regime which is observed on the PI signal corresponds to a modulation of the second decay discussed above in the PE spectra by 1.1 ps ($\sim$ 35 cm^{-1}) oscillations.

When considering the total PI signal of I-DTE-O_2, it appears that the contribution of numerous small fragments which are not (or poorly) modulated, is smoothing the oscillations and reducing their relative amplitude. This is a strong indication that the oscillations are associated with a periodic variation of the ionization efficiency as a function of the pump-probe time delay due to a modulation of the ionization cross section with the geometry of the molecule. This observation is consistent with the energy diagram in Figure 9 which shows that a quasi resonance for the 3-probe photon ionization of I-DTE-O_2 (middle panel) from the equilibrium geometry of the S_1 state ($S_{1,opt}$ in the figure) is not preserved at other geometries (for instance in the Franck-Condon region which is also shown in the Figure). Oscillation about the equilibrium geometry of the S_1 state thus likely results in a modulation of the ionization cross section. Unfortunately, it is difficult to discuss further the I-DTE-O_2 oscillations because of the scrambling effect that was revealed at the end of Section 4.2.2. The oscillations observed in the PI signal of I-DTE-O_3 are much more interesting because this scrambling effect is not at play.

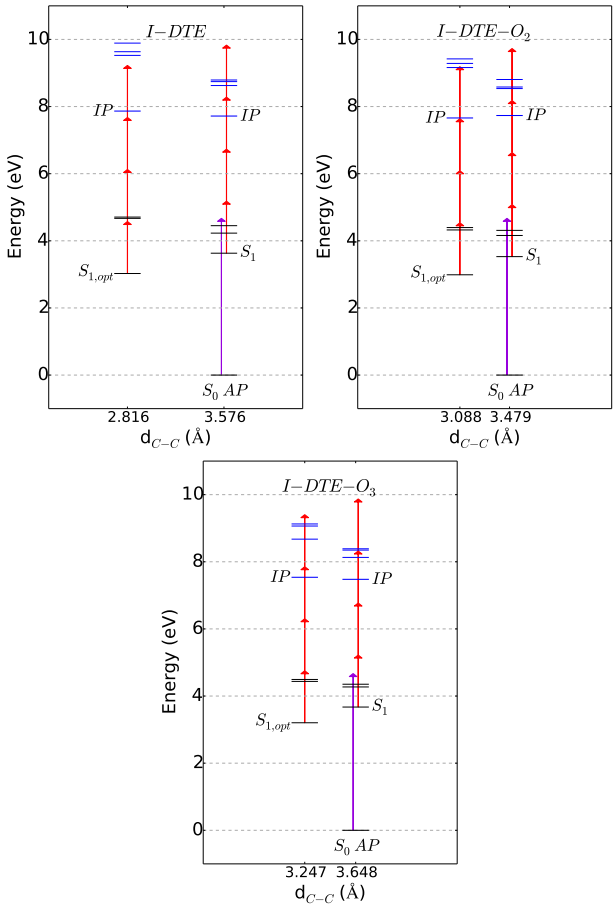

Fig. 9 Energy diagram of I-DTE, I-DTE-O_2 and I-DTE-O_3, made from data in Table 3. The purple arrows correspond to 265 photon (*i.e.* 4.67 eV), red arrows correspond to a 795 photon (*i.e.* 1.56 eV).

The energetics of the I-DTE-O_3 molecule is qualitatively similar to that of I-DTE-O_2, but significant quantitative differences exist, which prevent the ionization resonance mentioned above paragraph. In contrast a resonance exists in the ion which allows the absorption of a fourth probe photon at specific geometries. Hence, when the excited I-DTE-O_3 molecule oscillates about the equilibrium geometry of the S_1 state, it can be ionized by 4 or 3-probe photon whether this resonance is active or not. When the fourth photon is absorbed, enough energy is brought in the ion for fragmentation, hence transferring population from the parent ion to fragments. Since this

mechanism acts as a switch between parent and fragments, it is likely to generate the out-of-phase oscillations observed in Figure 8 between the I-DTE-O_3 parent and its fragment.

The oscillating regime observed in Figure 8 is damped with the same time constant as that of the second decay. Two mechanisms can be proposed for such coupled relaxation: i) direct vibronic relaxation to the ground state[42]; ii) coupling of the oscillating vibrational mode to deformation mode which targets the CI. In this latter case the vibrational coupling induces also a relaxation to the ground state but it is not direct and implies an intramolecular vibrational energy redistribution toward modes that are active regarding the photochromic reaction. Note that the situation is somehow different from the beating observed formally on cis-stilbene[43] or TDMAE[44], where vibrational modes orthogonal to the reaction pathway are populated.

In general, an oscillation regime occurs in a molecule when the wavepacket describing its vibrational motion overlaps several vibrational levels which beat together. These levels may belong to the same vibrational mode[45] or to different modes[24]. In the former case the 35 cm^{-1} energy which is associated with the 1.1 ps oscillation would correspond the mode energy, whereas in the second case it would correspond to the energy difference between the two modes. Both situations can be anticipated from calculations performed in the present work: the vibrational spectrum calculated at the $S_{1,opt}$ equilibrium geometry reveals indeed low energy modes that are consistent with the 35 cm^{-1} value; three modes also exist in the region of 1270-1370 cm^{-1}, which are separated by $\sim$ 35 cm^{-1}. Although no final answer can be given to determine which situation is at play, a tentative discussion can be given because the implication in terms of oscillation damping is not the same in both cases.

In the situation where the oscillations are due to the excitation of several quantas of a single large amplitude motion mode, the full vibrational wavepacket is also likely composed of modes which are higher in energy. Indeed, the excess energy provided by the excitation is *ca* 12,500 cm^{-1}, can hardly be fully accommodated by the low energy mode. Moreover, the energy stored in the low energy mode is probably not large enough to overcome the barrier toward the CI. Hence the observed decay of the electronic excitation is likely due to the coupling of one or several modes of higher energy with a coordinate targeting the CI. Alternatively a direct coupling with the ground state cannot be precluded. Since the oscillations within the low energy mode are damped at the same rate than the electronic excitation, this mode is essentially uncoupled to other modes, otherwise its decay would be faster.

In the second situation, where three high energy modes are populated coherently, the redistribution of the oscillations would be faster than that of the electronic excitation. Interestingly oscillations were also observed in the cyclereversion (ring opening) of 1,2-bis(2-methylbenzo[b]thiophen-3-yl)hexafluorocyclopentene (BTF6) in *n*-hexane[46]. This behavior is apparently similar to that observed in the present work, although it is not clear which vibrational mode is involved.

As a final remark, the fact that no oscillation appears in the PI signal of unbridged I-DTE molecule does not mean that no oscillating wavepacket is present in the excited state dynamics of this molecule. The bridge in the bridged molecules is not at the origin of the oscillation regime. Through its partial loss after ionization, it simply reveals that an oscillation regime exists within the molecule. Its absence in I-DTE precludes the observation of possible oscillation.

6 Conclusion

The relaxation dynamics of electronically excited photochromic inverse dithienylethene (I-DTE) derivatives was investigated by time-resolved photoelectron and photoion spectroscopy, using a velocity map imaging device and a time of flight mass spectrometer respectively. A femtosecond pump (@265 nm) - probe (@795 nm) arrangement coupled to beam setup was used in a scheme where the system under investigation, which is isolated in the gas phase, is probed by multiphoton ionization. Both the unbridged I-DTE molecule and three derivatives bridged by methoxy groups of various lengths were studied. The experimental results were complemented by first-principles calculations. Information on the low energy electronic states of these molecules, both in their neutral and ionized forms, at various geometries were provided by TD-DFT, whereas the ground-state structures have been sampled through molecular dynamics calculations.

We found that the electronic excitation decays with two time constants. This was not interpreted as a two step relaxation along a single reaction path as usual in femtochemistry. Instead, two parallel paths were assumed as suggested by calculations of the model diarylethenes molecules[10], after the initial wavepacket has split in two parts, each one having its own decay rate. The faster one (several femtoseconds) is assigned to the wavepacket relaxation through a conical intersection leading to the ground state of the closed form. The longer one (several picoseconds) is attributed to a relaxation of the other part of the wavepacket to the ground state through a vibronic coupling. The latter is either direct or indirect after intramolecular vibrational energy transfer has populated modes which are coupled to the CI. An oscillation regime is created by the pump laser excitation.

The central part of the present work is the splitting of the initial wavepacket which opens two parallel paths for the relaxation of the electronic excitation. Most probably, this situation applies to the whole family of dithienylethenes molecules and to other classes of molecules such as diarylethene and beyond.

Furthermore one can assume that in crystalline phase, the distortion of the molecules to reach the CI is not possible. The only mechanism being also available is the vibronic coupling. The condition for photochromism in the solide phase becomes also a condition on the relative location of the S_1 minimum and the barrier on the S_0 between the OF and CF.

Acknowledgments

L.P. thanks the ANR for support through the contract ANR-09-JCJC-0090-01 "CHROMADYNE". D.J. acknowledges the European Research Council (ERC) and the Région des Pays de la Loire for financial support in the framework of Starting Grants (Marches-278845) and a recrutement sur poste stratégique, respectively. This research used resources of the GENCI-CINES/IDRIS, of the CCIPL, and of a local Troy cluster. All authors are grateful to the GDRI-PHENICS international network. Furthermore, we thank the CEA/SLIC staff, in particular Olivier Gobert and Michel Perdrix, for technical support.

References

1 A. Stolow and J. Underwood, in *Time-resolved Photoelectron Spectroscopy Of Nonadiabatic Dynamics In Polyatomic Molecules*, ed. S. A. Rice, John Wiley & Sons Inc, New York, 2008, vol. 139, pp. 497–583.
2 H. Bouas-Laurent and H. Durr, *Pure Appl. Chem.*, 2001, **73**, 639–665.
3 M. Irie, *Chem. Rev.*, 2000, **100**, 1685–1716.
4 Y. Ishibashi, M. Fujiwara, T. Umesato, H. Saito, S. Kobatake, M. Irie and H. Miyasaka, *J. Phys. Chem. C*, 2011, **115**, 4265–4272.
5 M. Murakami, H. Miyasaka, T. Okada, S. Kobatake and M. Irie, *J. Am. Chem. Soc.*, 2004, **126**, 14764–14772.
6 S. Sangdeok, E. Intae, J. Taiha, K. Eunkyoung and K. S. Kwang, *J. Phys. Chem. A*, 2007, **111**, 8910–8917.
7 S. Kobatake and M. Irie, *Bull. Chem. Soc. Jap.*, 2004, **77**, 195–210.
8 M. Morimoto, S. Kobatake and M. Irie, *J. Am. Chem. Soc.*, 2003, **125**, 11080–11087.
9 S. Aloise, M. Sliwa, G. Buntinx, S. Delbaere, A. Perrier, F. Maurel, D. Jacquemin and M. Takeshita, *Phys. Chem. Chem. Phys.*, 2013, **15**, 6226–6234.
10 M. Boggio-Pasqua, M. Ravaglia, M. J. Bearpark, M. Garavelli and M. A. Robb, *J. Phys. Chem. A*, 2003, **107**, 11139–11152.
11 M. J. Bearpark, M. Deumal, M. A. Robb, T. Vreven, N. Yamamoto, M. Olivucci and F. Bernardi, *J. Am. Chem. Soc.*, 1997, **119**, 709–718.
12 F. Bernardi, M. Olivucci and M. A. Robb, *J. Photochem. Photobiol. A*, 1997, **105**, 365–371.
13 A. Perrier, S. Aloise, M. Olivucci and D. Jacquemin, *J. Phys. Chem. Lett.*, 2013, **4**, 2190–2196.
14 S. Aloise, M. Sliwa, Z. Pawlowska, J. Rehault, J. Dubois, O. Poizat, G. Buntinx, A. Perrier, F. Maurel, S. Yamaguchi and M. Takeshita, *J. Am. Chem. Soc.*, 2010, **132**, 7379–7390.
15 N. Tamai, T. Saika, T. Shimidzu and M. Irie, *J. Phys. Chem.*, 1996, **100**, 4689–4692.
16 S. Kobatake, K. Uchida, E. Tsuchida and M. Irie, *Chem. Commun.*, 2002, 2804–2505.
17 H. Jean-Ruel, R. R. Cooney, M. Gao, C. Lu, M. A. Kochman, C. A. Morrison and R. J. D. Miller, *J. Phys. Chem. A*, 2011, **115**, 13158–13168.
18 M. Takeshita, C. Tanaka, T. Miyazaki, Y. Fukushima and M. Nagai, *New J. Chem.*, 2009, **33**, 1433–1438.
19 M. Takeshita, M. Nagai and T. Yamato, *Chem. Commun.*, 2003, 1496–1497.
20 H. Jin-nouchi and M. Takeshita, *Chem. Eur. J.*, 2012, **18**, 9638–9644.
21 Y. Tatsumi, J.-i. Kitai, W. Uchida, K. Ogata, S. Nakamura and K. Uchida, *J. Phys. Chem. A*, 2012, **116**, 10973–10979.
22 K. Uchida, H. Sumino, Y. Shimobayashi, Y. Ushiogi, A. Takata, Y. Kojima, S. Yokojima, S. Kobatake and S. Nakamura, *Bull. Chem. Soc. Jap.*, 2009, **82**, 1441–1446.
23 L. Poisson, K. D. Raffael, B. Soep, J.-M. Mestdagh and G. Buntinx, *J. Am. Chem. Soc.*, 2006, **128**, 3169–3178.
24 L. Poisson, R. Maksimenska, B. Soep, J.-M. Mestdagh, D. H. Parker, M. Nsangou and M. Hochlaf, *J. Phys. Chem. A*, 2010, **114**, 3313–3319.
25 A. T. Eppink and D. H. Parker, *Rev. Sci. Instrum.*, 1997, **68**, 3477–3484.
26 G. A. Garcia, L. Nahon and I. Powis, *Rev. Sci. Instrum.*, 2004, **75**, 4989–4996.
27 L. Poisson, *LV_pBASEX*, 2009.
28 L. Poisson, P. Roubin, S. Coussan, B. Soep and J.-M. Mestdagh, *J. Am. Chem. Soc.*, 2008, **130**, 2974–2983.
29 S. Awali, L. Poisson, B. Soep, M. A. Gaveau, M. Briant, C. Pothier, J. M. Mestdagh, M. Ben El Hadj Rhouma, M. Hochlaf, V. Mazet and S. Faisan, *Phys. Chem. Chem. Phys.*, 2013, **16**, 516–526.
30 M. J. Frisch, G. W. Trucks, H. B. Schlegel, G. E. Scuseria, M. A. Robb, J. R. Cheeseman, G. Scalmani, V. Barone, B. Mennucci, G. A. Petersson, H. Nakatsuji, M. Caricato, X. Li, H. P. Hratchian, A. F. Izmaylov, J. Bloino, G. Zheng, J. L. Sonnenberg, M. Hada, M. Ehara, K. Toyota, R. Fukuda, J. Hasegawa, M. Ishida, T. Nakajima, Y. Honda, O. Kitao, H. Nakai, T. Vreven, J. J. A Montgomery, J. E. Peralta, F. Ogliaro, M. Bearpark, J. J. Heyd, E. Brothers, K. N. Kudin, V. N. Staroverov, R. Kobayashi, J. Normand, K. Raghavachari, A. Rendell, J. C. Burant, S. S. Iyengar, J. Tomasi, M. Cossi, N. Rega, J. M. Millam, M. Klene, J. E. Knox, J. B. Cross, V. Bakken, C. Adamo, J. Jaramillo, R. Gomperts, R. E. Stratmann, O. Yazyev, A. J. Austin, R. Cammi, C. Pomelli, J. W. Ochterski, R. L. Martin, K. Morokuma, V. G. Zakrzewski, G. A. Voth, P. Salvador, J. J. Dannenberg, S. Dapprich, A. D. Daniels, O. Farkas, J. B. Foresman, J. V. Ortiz, J. Cioslowski and D. J. Fox, *Gaussian 09 Revision A2*, 2009.
31 D. Jacquemin, A. Planchat, C. Adamo and B. Mennucci, *J. Chem Theory Comput.*, 2012, **8**, 2359–2372.
32 J.-D. Chai and M. Head-Gordon, *J. Chem. Phys.*, 2008, **128**, year.
33 N. Mardirossian, J. A. Parkhill and M. Head-Gordon, *Phys. Chem. Chem. Phys.*, 2011, **13**, 19325–19337.
34 M. Ernzerhof and G. Scuseria, *J. Chem. Phys.*, 1999, **110**, 5029–5036.
35 C. Adamo and V. Barone, *J. Chem. Phys.*, 1999, **110**, 6158–6170.
36 A. Fihey, A. Perrier and F. Maurel, *J. Photochem. Photobiol. A*, 2012, **247**, 30–41.
37 A. D. Laurent, J.-M. Andre, E. A. Perpete and D. Jacquemin, *J. Photochem. Photobiol. A*, 2007, **192**, 211–219.
38 J. M. Mestdagh, J.-P. Visticot, M. Elhanine and B. Soep, *J. Chem. Phys.*, 2000, **113**, 237–248.
39 A. Frad, F. Lahmani, A. Tramer and C. Tric, *J. Chem. Phys.*, 1974, **60**, 4419–4430.
40 L. Poisson, P. Pradel, F. Lepetit, F. Reau, J. M. Mestdagh and J. P. Visticot, *EPJ D*, 2001, **14**, 89–95.
41 L. Poisson, L. Dukan, O. Sublemontier, F. Lepetit, F. Reau, P. Pradel, J. M. Mestdagh and J. P. Visticot, *Int. J. Mass Spectrom.*, 2002, **220**, 111–126.
42 J. Jortner, R. D. Levine and S. A. Rice, in *Level Structure and Dynamics from Diatomics to Clusters*, 1988, vol. 70, pp. 1–34.
43 S. Pedersen, L. Baares and A. H. Zewail, *The Journal of Chemical Physics*, 1992, **97**, 8801–8804.
44 E. Gloaguen, J. Mestdagh, L. Poisson, F. Lepetit, J. Visticot, B. Soep,

M. Coroiu, A. Eppink and D. Parker, *J. Am. Chem. Soc.*, 2005, **127**, 16529–16534.

45 P. Cong, G. Roberts, J. Herek, A. Mohktari and A. Zewail, *J. Phys. Chem.*, 1996, **100**, 7832–7848.

46 H. Miyasaka, M. Murakami, T. Okada, Y. Nagata, A. Itaya, S. Kobatake and M. Irie, *Chem. Phys. Lett.*, 2003, **371**, 40–48.